Quantifying the Impact of Declustering Techniques on Completeness Magnitude Estimation

Massimiliano Guastella*[1,2], Anna Figlioli[2], Raffaele Martorana[3,4], and Antonino D'Alessandro[4]

ABSTRACT

OPEN ACCESS

Seismicity analysis and earthquake hazard assessment require catalogs of independent events and accurate estimates of completeness. The magnitude of completeness (M_c) defines the threshold below which earthquakes are likely to be missed; declustering, used to remove dependent events, can substantially alter M_c by reshaping the lower tail of the frequency–magnitude distribution. Because such changes propagate to the Gutenberg–Richter *b*-value, method choices may bias downstream analyses. Using a regional instrumental catalog from southern Italy, we try to quantify how widely used declustering approaches affect catalog-based estimates of M_c. We apply three declustering families: fixed window (Gardner and Knopoff original formulation, including Gruenthal and Uhrhammer windows), linked window (Reasenberg, three parameter configurations), and nearest neighbor. Then we estimate M_c with five catalog-based methods: maximum curvature, goodness-of-fit test, median-based analysis of segment slope, entire magnitude range, and magnitude of completeness by *b*-value stability. Comparing across declustered and observed catalogs, we evaluate how declustering event removal modifies the frequency–magnitude distribution and in turn the sensitivity of catalog-based M_c methods to these modifications. Resampling is used to assess precision and stability, the results remain essentially unchanged even with small bootstrap sizes, indicating the need but large numbers of resamples are unnecessary. Overall, the analysis highlights that declustering choice and completeness estimation are critical decisions and should be reported jointly when deriving the *b*-value for seismic hazard applications.

KEY POINTS

- Declustering alters the shape of the frequency–magnitude distribution.
- Completeness estimates sensitivity to the choice of declustering technique.
- Bootstrap resampling identifies over- and underestimation in standalone M_c estimates.

INTRODUCTION

Earthquake catalogs are important datasets to understand seismicity, earthquake physics, and earthquake hazard (Huang *et al.*, 1994; Liu *et al.*, 1996; Xu and Gao, 2014). Catalogs provide valuable information about the occurrence, location, and magnitude of earthquakes over a specific time period. The standard probabilistic seismic hazard analysis (PSHA) framework treats earthquake occurrence as a stationary Poisson process, implying that the probability of a future event is independent of the history of previous events within the same source zone (Cornell, 1968). Earthquake declustering is the process of removing dependent events from a seismic catalog so that only independent events remain. A not declustered catalog can bias frequency–magnitude statistics and hazard estimates by inflating event counts in clustered periods or regions. Consequently, best practices in seismic analysis recommend carefully choosing the declustering procedure and exploring multiple methods to estimating hazard parameters (Luen and Stark, 2012; Taroni and Akinci, 2021). At present, many algorithms are available for declustering

1. Dipartimento d'Ingegneria Civile ed Ambientale, Università Sapienza, Rome, Italy, https://orcid.org/0009-0006-9841-6275 (MG); 2. Dipartimento di Scienze della Terra e del Mare, Università degli studi di Palermo, Palermo, Italy, https://orcid.org/0000-0002-5101-6788 (AF); 3. Sezione di Milano, Istituto Nazionale di Geofisica e Vulcanologia, Milan, Italy, https://orcid.org/0000-0002-4421-9501 (RM); 4. Osservatorio Nazionale dei Terremoti, Istituto Nazionale di Geofisica e Vulcanologia, Rome, Italy, https://orcid.org/0000-0002-0074-3125 (AD)

*Corresponding author: massimiliano.guastella@uniroma1.it

Cite this article as Guastella, M., A. Figlioli, R. Martorana, and A. D'Alessandro (2026). Quantifying the Impact of Declustering Techniques on Completeness Magnitude Estimation, *Bull. Seismol. Soc. Am.* **116**, 946–962, doi: 10.1785/0120250144

earthquake catalogs. These approaches range from longstanding simple window-based methods to newer statistically adaptive formulations, each embedding different assumptions about spatiotemporal triggering and parameterization. Consequently, declustered outcomes are method dependent, and no single procedure is universally preferred as shown in many studies (Amini, 2014; Azak *et al.*, 2018; Taroni and Akinci, 2021; Juellyan *et al.*, 2023; Perry and Bendick, 2024).

Another core aspect of hazard analysis is the completeness magnitude (M_c). This threshold magnitude represents the lower limit of earthquake magnitudes that can be reliably detected and recorded by the seismic network. Any earthquake with a magnitude below this threshold may either go unnoticed or be underrepresented in the catalog (Rydelek and Sacks, 1989). Accurate estimation of completeness allows researchers to obtain reliable statistical analysis and interpretation of earthquake patterns and behavior (Mignan and Woessner, 2012). However, it is widely recognized that earthquake catalogs are inherently incomplete, meaning that they do not capture the full extent of seismic activity in a given area. This incompleteness stems from various factors, including instrumental limitations, network coverage, data processing techniques, and the influence of natural phenomena on earthquake detection. Furthermore, the occurrence of large-magnitude earthquakes may lead to a decreased number of detected earthquakes in the immediate aftermath. This can often be attributed to the "blind time" immediately after a large seismic event, when seismic networks miss smaller successive events because of the saturation of seismic sensors and the general high level of seismic noise (Kagan, 2004; Helmstetter *et al.*, 2006). This blind time produces an increase in the completeness of the catalog because of the loss of data during a seismic sequence. In addition, the spatial distribution of seismic monitoring networks contributes to catalog incompleteness. Uneven network coverage, particularly in remote or inaccessible regions, can lead to gaps in earthquake detection and reporting. Sparse monitoring stations in certain areas result in reduced seismic data availability, leading to incomplete catalogs for these regions (Schorlemmer *et al.*, 2010; Abd el-aal, 2012; Mignan and Chouliaras, 2014; Gonzalez, 2017; D'Alessando *et al.*, 2021).

Data processing techniques also play an important role in catalog completeness. Signal processing algorithms and filtering methods applied to raw seismic data can introduce biases and affect the detection and identification of earthquakes, particularly in case of small-magnitude events. Under these circumstances, the selection of appropriate processing parameters is crucial to optimize event detection and minimize data loss. Furthermore, natural phenomena can have an impact on a catalog's completeness. High levels of background noise from environmental factors, such as oceanic waves, cultural noise, or anthropogenic activities, can also mask or obscure seismic signals. In a wide range of magnitudes within seismogenic zones, the distribution of earthquake sizes can typically be effectively represented through a power law relationship (Abercrombie, 1995).

There are primarily two approaches to estimating the completeness magnitude: (1) catalog-based methods, which rely solely on catalog data, and (2) waveform-based methods. These latter methods have been exemplified in studies by Sereno and Bratt (1989) and Gomberg (1991). Waveform-based methods that require estimating the signal-to-noise ratio for numerous events at many stations are time-consuming and cannot generally be performed as part of a particular seismicity study (Wiemer and Wyss, 2000). In the vast majority of instances, methods relying on catalogs ascertain the M_c-value by identifying the threshold beneath which the cumulative frequency–magnitude distribution (FMD) diverges from the Gutenberg–Richter (G-R) law (Gutenberg and Richter, 1944). The G-R law, shown in equation (1), models the relationship between earthquakes magnitudes and their frequencies in a given area. It states that the logarithm of the number of earthquakes with magnitude greater than or equal to a given value decreases linearly with that magnitude. This relationship is quantified by a characteristic parameter known as the b-value, which represents the relative frequency of small to large earthquakes (Ishimoto and Iida, 1939; Gutenberg and Richter, 1944). Mathematically, it can be expressed as

$$\log(N) = a - b(M - M_{\min}), \tag{1}$$

in which N represents earthquakes with a magnitude greater than or equal to a specific magnitude (M_w), a and b are the parameters of the G-R law, and M_{min} represents the lower magnitude cutoff used to fit the relation. The a-value, or "b-value intercept," reflects the seismicity rate at a specific magnitude. A higher a-value suggests a higher level of seismic activity, and a lower value indicates relatively fewer earthquakes. The b-value, or slope parameter, is a core parameter for hazard analysis. It characterizes the relative distribution of earthquake magnitudes: a high b-value indicates a larger proportion of small earthquakes, a lower b-value indicates a larger proportion of large earthquakes (Schorlemmer *et al.*, 2005). In most catalog-based methods, M_c is inferred from the expected behavior of seismicity by fitting a G-R model to the observed FMD (Mignan and Woessner, 2012). In the context of the G-R law, the magnitude at which the lower end of the observed FMD departs from the G-R model is taken as an estimate of M_c (Zuniga and Wyss, 1995).

The observed catalog shows a gradual curvature. This kind of model has been explained by different formulations of the detection function, including the cumulative normal distribution, also called the error function (ERF) (Ringdal, 1975; Ogata and Katsura, 1993; Ogata and Katsura, 2006). The ERF model uses the parameters μ and σ to describe this gradual curvature. Here, μ represents the mean detection threshold magnitude, indicating the central point of the detection function, whereas

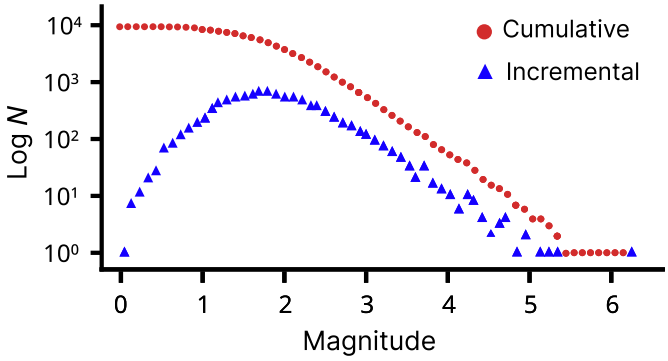

Figure 1. Synthetic gradually curved frequency–magnitude distribution (FMD) based on the error function (ERF) model (Ringdal 1975; Ogata and Katsura, 2006), with parameters $\mu = 2.0$ and $\sigma = 0.5$. The color version of this figure is available only in the electronic edition.

σ represents the standard deviation, indicating the spread or variability of the detection probabilities around this mean (Fig. 1). In the context of this model, the incremental FMD is characterized by a gradual curvature below the completeness magnitude and indicates that smaller earthquakes are less likely to be detected compared with larger ones. Understanding the FMD shape and how declustering alters it are essential aspects to obtain reliable and meaningful results. Declustering acts by filtering events as well as the completeness magnitude, although on a different basis. The balance between necessities of the study and sample size should be always pursued. It is also suggested a visual inspection of the curvature to help evaluate the performance of different M_c and avoid relying exclusively on numeric results (Mignan and Woessner, 2012). In this study, we aim to quantify the sensitivity of catalog-based estimates of M_c by comparing results obtained from the observed catalog with declustered catalogs generated using different algorithms.

MATERIALS AND METHODS

The seismic catalog (Fig. 2), provided by Istituto Nazionale di Geofisica e Vulcanologia (INGV), covers a range of 18 yr from 2005 to 2022. It comprises a comprehensive record of 26.300 earthquakes that occurred within this timeframe. The catalog encompasses a wide range of magnitudes, starting from 0.1 and reaching a maximum magnitude of 5.8. Geographically, it captures seismic activity in the region of Sicily, Italy, with coverage extending from longitude 11.6420 E to 16.4700 E and latitude 35.0020 N to 39.6957 N. Figure 3 depicts a heatmap showcasing the distribution of earthquakes frequencies for the observed catalog, classified in 0.5 yr interval and 0.1 magnitude increments. The highest concentration of event lies between 1.8 and 2.6;counts decrease rapidly for $M \geq 3.5$ and $M \leq 1.0$. We used three widely adopted algorithms that rely on different assumptions. The first declustering algorithm used is the Gardner and Knopoff window approach, extended with the Gruenthal and Uhrhammer variants (Gardner and Knopoff, 1974; Uhrhammer, 1986; Van Stiphout *et al.*, 2012). The Reasenberg linked-window method (Reasenberg, 1985) with the three parameters configuration reported by Van Stiphout *et al.* (2012). Finally, we applied the nearest-neighbor approach to make comparisons with more recent algorithms (Zaliapin and Ben-Zion, 2020). A total of eight catalogs were produced, including the observed not declustered catalog, and they were analyzed using five catalog-based methods to estimate the magnitude of completeness: maximum curvature (MAXC) (Wyss *et al.*, 1999, Wiemer and Wyss, 2000), goodness-of-fit test (GFT) (Wiemer and Wyss, 2000), median-based analysis of segment slope (MBASS) (Amorese, 2007), entire magnitude range (EMR) (Woessner and Wiemer, 2005), and magnitude of completeness by *b*-value stability (Cao and Gao, 2002). This analytical design enables a direct assessment of the sensitivity of M_c to the different decluster settings used. Method-specific uncertainties were quantified via bootstrap resampling using 500, 1000, 2000, and 3000 replicates for each catalog–method combination. A simulation analysis was conducted using synthetically generated catalogs to delve into the differences between the results obtained from M_c estimates in the observed catalog. Because of the gradually curved shape of the studied FMD, synthetic catalogs were based on the ERF model parameters. Magnitude of completeness computational calculations were performed using the statistical software R based on Mignan and Woessner (2012) and Amorese (2007). In addition, simulation analysis was conducted using the rseismNet R package. The declustering operations, for which the python software were used, were carried out using the OpenQuake Engine package by the Global Earthquake Modeling Foundation. (Silva *et al.*, 2014).

Declustering algorithms

Declustering a seismic catalog typically yields two products: a copy of the original catalog in which each event is classified according to the chosen algorithm and a subcatalog containing only events considered independent. Although these algorithms act on different decision rules, they both filter events in a way that can interact with M_c. In this study, we applied the fixed-window Gardner and Knopoff declustering algorithm with the variant space–time windows of Gruenthal and Uhrhammer (Gardner and Knopoff, 1974; Uhrhammer, 1986; Van Stiphout *et al.*, 2012). To extend the comparison beyond fixed windows, we also used the linked-window Reasenberg algorithm (Reasenberg, 1985) with three parameter configurations described in practice following Van Stiphout *et al.* (2012) and the newer emerging nearest-neighbor approach, which identifies clusters via a proximity metric in space–time–magnitude (Zaliapin and Ben-Zion, 2020). This allowed us to explore method-parameter-dependent variability of declustering outcomes on the Sicilian catalog.

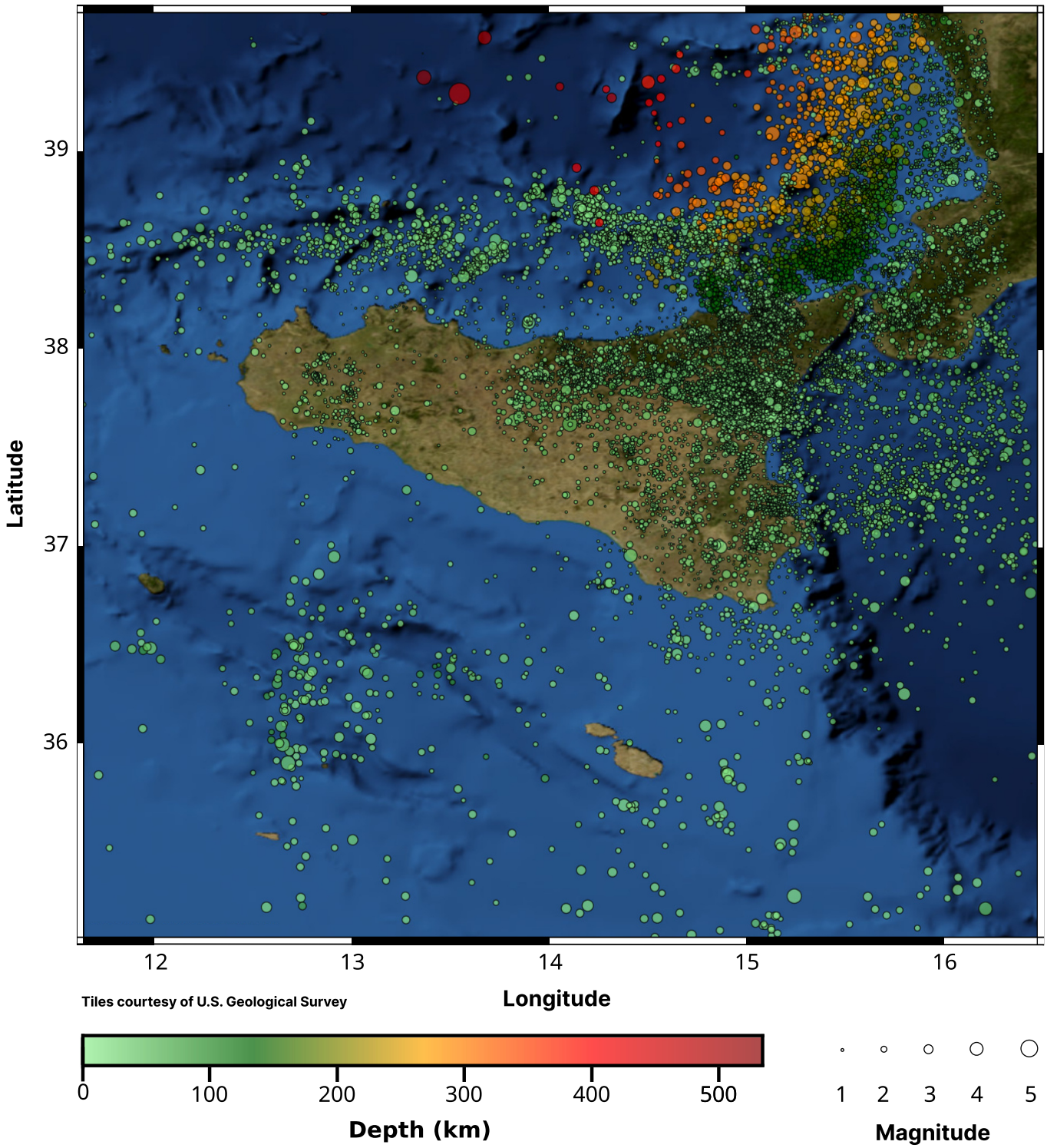

Figure 2. Events spatial distribution of the analyzed seismic catalog (2005–2022). The color version of this figure is available only in the electronic edition.

Gardner and Knopoff approach

One of the earliest and still widely used approaches is the Gardner and Knopoff algorithm (Gardner and Knopoff, 1974). It belongs to the family of windowing techniques that separate dependent from independent events by applying magnitude-dependent fixed windows in time and space. In practice, for each earthquake, a temporal window and a spatial radius are defined as functions of its magnitude, and any event occurring within the bounds set by a larger event is classified as a dependent and removed from the background. Different space–time windows have been proposed in the literature, each

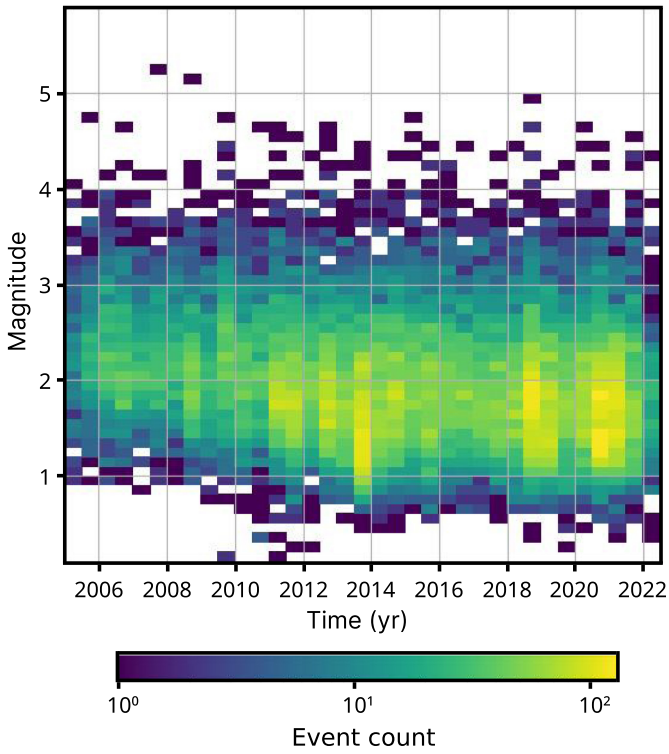

Figure 3. Observed seismic event density over time (year and magnitude bin size, respectively, are equal to 0.5 and 0.1). The color version of this figure is available only in the electronic edition.

empirically calibrated on specific regional seismicity. The original coefficients by Gardner and Knopoff are calibrated on southern California seismicity (Gardner and Knopoff, 1974), whereas the alternative parameter sets proposed by Gruenthal and by Uhrhammer are based on regional catalogs of Central Europe and northern–central California, respectively (Uhrhammer, 1986; Van Stiphout *et al.*, 2012). As shown in equations (2)–(4), each windowing formulation defines magnitude-dependent thresholds that govern how closely spaced events are considered dependent:

$$\begin{aligned}\text{Distance (Gardner and Knopoff)} &= 10^{0.1238M+0.983}\,(\text{km})\\ \text{Time (Gardner and Knopoff)} &= 10^{0.5409M-0.547}\,(\text{days}),\end{aligned} \tag{2}$$

$$\begin{aligned}\text{Distance (Gruenthal)} &= e^{1.77+(0.037+1.02M)^2}\,(\text{km})\\ \text{Time (Gruenthal)} &= 10^{2.8+0.024M}\,(\text{days}),\end{aligned} \tag{3}$$

$$\begin{aligned}\text{Distance (Uhrhammer)} &= e^{-1.024+0.804M}\,(\text{km})\\ \text{Time (Uhrhammer)} &= e^{-2.87+1.235M}\,(\text{days}).\end{aligned} \tag{4}$$

Because of maximum magnitude observed in the original catalog does not reach the magnitude threshold set by the authors, the Gardner and Knopoff and Gruenthal time window definitions for $M \geq 6.5$ are not reported as not needed. This declustering algorithm consists of an iterative process that involves the following steps:

1. The earthquakes are sorted in descending order according to magnitude and initially considered as potential mainshocks.
2. The iteration starts, and each event is evaluated individually to determine if it meets the criteria to be classified as a mainshock, foreshock, or aftershock.
3. The first event corresponds to the maximum magnitude value in the catalog, meaning that it is a mainshock.
4. When a mainshock is detected, the time–space window is applied both forward and backward. At this point, an assessment is made to determine if other events fall within the spatial temporal distance defined by the window. If an earthquake satisfies the distance criterion and falls within the time window of a larger event, it is labeled as an aftershock or foreshock.
5. The process resumes from the last labeled mainshock event, repeating the procedure until all events in the series have been classified.

Reasenberg approach

Reasenberg implements a linked-window method in which each event opens a time–space interaction window, and any subsequent event that falls within is linked and in turn opens its own window so that clusters grow transitively (Reasenberg, 1985). The temporal parameters ($\tau_{\min}$,$\tau_{\max}$) delimit the admissible bounds of the prospective look-ahead time τ. For a target detection probability p_1, τ is calculated as shown in equation (5),

$$\tau = -\ln(1-p_1)t10^{-\frac{2}{3}(\Delta M-1)}, \tag{5}$$

in which $\Delta M = M_{max} - x_{meff}$ is the magnitude contrast between the current largest event and the membership threshold in magnitude x_{meff} and t is a timescale constant. The value from equation (5) is then truncated to [$\tau_{\min}$,$\tau_{\max}$]. The interaction distance follows the spatial criterion well summarized in Molchan and Dmitrieva (1992) and shown in equation (6),

$$\log_{10} d(\text{km}) = 0.4M_0 - 1.943 + k, \tag{6}$$

in which d is the maximum separation for linkage, M_0 is the magnitude of the reference event, and $k \in \{0,1\}$ switches between using the distance to the last linked event ($k = 0$) or to the largest event currently in the cluster ($k = 1$). In addition, x_k controls how strongly the effective lower magnitude cutoff is raised during an active sequence via $x_{\text{eff}} = x_{meff} + x_k M_{\max}$; a larger x_k means a higher cutoff, and therefore fewer small events are linked. Finally, r_{fact} is the scale factor that sets the spatial neighborhood (Kanamori and Anderson, 1975); a larger r_{fact}

TABLE 1
Parameter Configuration Used for the Reasenberg Declustering Algorithm, Including Standard Values and Parameter Ranges Described by Van Stiphout *et al.* (2012)

Parameter	Standard	Min	Max
τ_{min} (days)	1	0.5	2.5
τ_{max} (days)	10	3	15
p	0.95	0.9	0.99
x_k	0.5	0	1
x_{meff}	1.5	1.6	1.8
r_{fact}	10	5	20

widens the spatial window, allowing more permissive linking, whereas smaller values tighten it, leading to a more conservative linking. Even though the parameter choices often follow the standard setting (Van Stiphout *et al.*, 2012), we decided to also use the minimum and maximum configurations (Schorlemmer and Gerstenberger, 2007) summarized in Table 1:

1. The earthquakes are sorted in chronological order and initially left unassigned as potential cluster seeds.
2. Starting from the first unassigned event, define its interaction zone by a look-ahead time window and a magnitude-dependent spatial distance threshold.
3. Scan forward in time and link any subsequent event that falls within both the temporal and spatial criteria to the current cluster; each linked event opens its own interaction zone and can link further events.
4. When no additional links are found, close the cluster, designate the largest-magnitude member as the mainshock, and label earlier members as foreshocks and later members as aftershocks.
5. Mark all cluster members as assigned and continue from the next unassigned event until the entire catalog is processed; obtain the declustered catalog by retaining mainshocks only.

Nearest-neighbor approach

The nearest-neighbor approach constructs a directed tree by assigning to each earthquake j a single nearest predecessor $i < j$ within a joint space–time–magnitude proximity (Zaliapin and Ben-Zion, 2013a,b; Zaliapin and Ben-Zion, 2020). The core quantity is the proximity between two events (equation 7), which combines interevent time, spatial separation, and a magnitude weighting consistent with Gutenberg–Richter statistics:

$$\eta_{ij} = t_{ij} r_{ij}^{d}\, 10^{-w m_i}, \tag{7}$$

in which $t_{ij} = t_j - t_i$ is the interevent time; r_{ij} is the epicentral distance between the events; m_i is the magnitude of the potential parent i; w, and d control, respectively, the magnitude weighting and the spatial scaling. Following the declustering recommendations of Zaliapin and Ben-Zion (2020), we work with epicenters only and set $w = 0$ and $d = 1.5$.

Each event is linked to its nearest-neighbor in this proximity,

$$i^*(j) = \arg\min_{i<j} \eta_{ij}, \tag{8}$$

and the link strength is summarized by

$$\xi_j = \log_{10}(\eta_{i^*(j)j}). \tag{9}$$

A data-driven cutoff on ξ_j (equivalently, $\xi_j \le \log_{10}\eta_0$), estimated from the empirical typically bimodal distribution of ξ_j, separates clustered from background links:

$$\text{Link}(j) = \begin{cases} \text{Clustered} & \text{if } \xi_j \le \log_{10}\eta_0, \\ \text{Background} & \text{if } \xi_j > \log_{10}\eta_0. \end{cases} \tag{10}$$

1. For each earthquake, compute its proximity to every earlier earthquake, assign as parent the earlier event with the smallest proximity, and record the base-10 logarithm of that minimum proximity as the link strength.
2. Using a data-driven cutoff derived from the empirical distribution of link strengths, classify each parent–child link as either clustered or background and retain only the clustered links.
3. From the retained links, identify connected groups (families); within each family, designate the largest-magnitude event as the mainshock, label events that occur before it as foreshocks, and label those that occur after it as aftershocks.
4. Apply random thinning based on the normalized score with a single global threshold; the retained events form the declustered catalog.

CATALOG-BASED METHODS TO ESTIMATE THE COMPLETENESS MAGNITUDE

MAXC

The MAXC technique (Wyss *et al.*, 1999; Wiemer and Wyss, 2000) is a catalog-based method used to estimate the magnitude of completeness in earthquake catalogs. It operates by calculating the maximum value of the first derivative of the frequency–magnitude curve. In practical terms, this method identifies the magnitude that corresponds to the mode of the noncumulative FMD. By identifying the magnitude associated with the highest frequency of events in the FMD, it aims to capture a significant point of deviation from the linear cumulative part of the Gutenberg–Richter law.

GFT

The GFT method, developed by Wiemer and Wyss (2000), is a parametric method used to assess quantitatively the differences

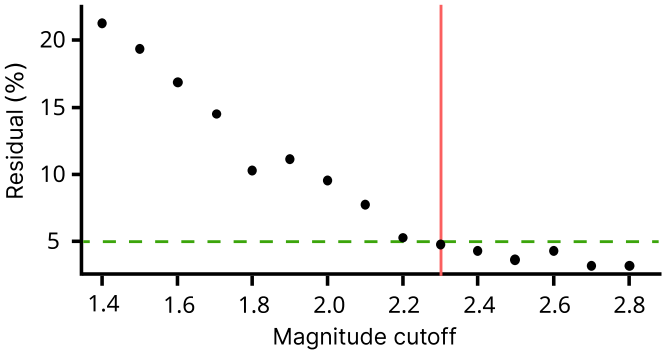

Figure 4. Goodness-of-fit test (GFT) method: residual are plot as a function of magnitude cutoff interval. The completeness is identified (vertical line) as the first value that achieve the confidence level (dashed horizontal line). The color version of this figure is available only in the electronic edition.

between the observed and synthetic distributions, providing a measure of how well the G-R law fits the input data. The procedure begins by selecting a magnitude cutoff range, which represents the potential magnitude of completeness values. The G-R law is then applied to calculate the theoretical distribution of earthquake magnitudes using maximum-likelihood estimation of the parameters a and b from the observed data. The next step involves comparing the observed cumulative number of events (Bi) in each M_{co} with the predicted cumulative number of events (Si) from the theoretical distribution. The absolute difference R between Bi and Si is calculated for each magnitude cutoff using the equation (11):

$$R(a,b,M_{co}) = 100 - \left(\frac{\sum_{M_{co}}^{M_{\max}} |B_i - S_i|}{\sum_i B_i} 100\right). \qquad (11)$$

By evaluating R at different magnitude thresholds, the test identifies the M_c-value that satisfies the desired confidence level. If the observed and theoretical distributions exhibit large differences, indicating a poor fit, a higher M_c-value will be selected. Conversely, if the observed and theoretical distributions align well, the M_c-value will be lower.

The completeness magnitude is defined as the first magnitude cutoff at which the residual falls below the horizontal line corresponding to the desired confidence level (e.g., 95% fit) as presented in Figure 4. If the desired confidence level cannot be achieved, 90% may be used as a compromise. If even the 90 confidence level cannot be reached, the MAXC estimate is used instead.

MBASS

Amorese (2007) introduced the MBASS method as a nonparametric technique for estimating the magnitude of completeness in earthquake catalogs. It is based on the change-point detection principles to identify multiple discontinuities in the incremental FMD, with the primary discontinuity corresponding to completeness. The MBASS method builds on the multiple change-point procedure developed by Lanzante (1996), which has demonstrated success in climate data analysis by employing resistant, solid, and nonparametric approach. In the context of earthquake catalog, the MBASS algorithm follows an iterative process to estimate M_c. Initially, the FMD is divided into segments, defined by magnitude cutoffs. For each segment, the slope is calculated and then iteratively tested for change points, representing potential M_c-values. The null hypothesis states that the frequencies are equal. The acceptance or rejection of the null hypothesis of no change at the identified change point is based on the Wilcoxon–Mann–Whitney test (Wilcoxon, 1945), a widely used nonparametric statistical test. The significance level for evaluating the statistical significance of each change point is typically chosen in advance. In this study, a significance level of 5 has been chosen. The change-point test is iteratively applied to the magnitude series as long as the statistical significance of each new change point remains below the specified significance level. Each iteration generates a list of $N + 1$ change points, and prior to applying the change-point test in subsequent iterations, the magnitude series is adjusted by subtracting the median of each segment slope from the corresponding points. The final M_c estimate is determined based on the identified change points, typically using the magnitude associated with the best test statistic as the M_c-value which corresponds to the main discontinuity. Figure 5 depicts the identification of the main discontinuity obtained through 3000 bootstrap sample for the observed catalog. Other discontinuities may correspond to upper-magnitude breakpoints (Wesnousky, 1994). The MBASS procedure cannot be applied to cumulative FMD data because, in common with many other statistical procedures, the Wilcoxon–Mann–Whitney test requires independence within groups (Hollander and Wolfe, 1973).

EMR

The EMR method (Woessner and Wiemer, 2005) offers a parametric approach to estimating the completeness magnitude using a two-part model that combines the Gutenberg–Richter law and a cumulative normal distribution function. This method accounts for both the complete and incomplete parts of the magnitude–frequency distribution. In the EMR model, the first component of the model incorporates the G-R law and represents the part of the earthquake catalog in which earthquake detection is assumed to be reliable and complete, capturing the entirety of seismic activity above the completeness. The second component of the model incorporates a cumulative normal distribution function, denoted as q, which characterizes the detection capability of the seismic network. This component addresses the incomplete part in the catalog, modeling the incremental frequency magnitude below M_c, acknowledging that some events might not be

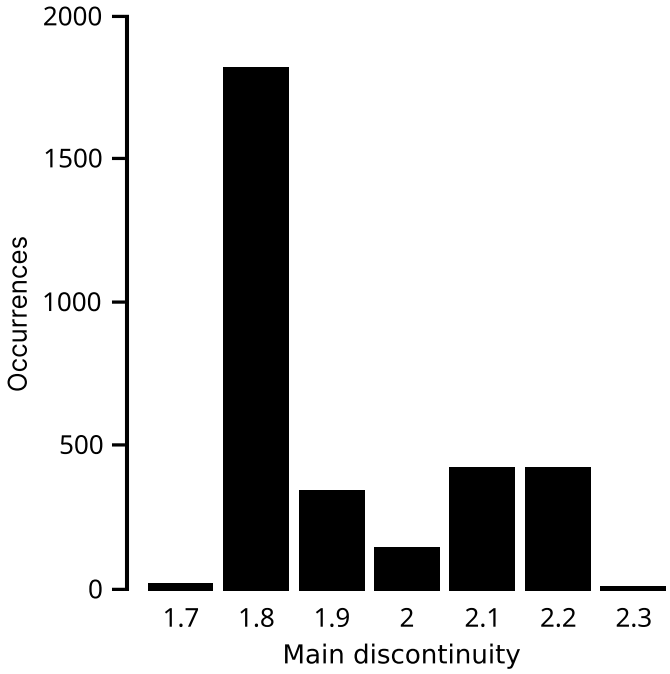

Figure 5. Median-based analysis of the segment slope method (MBASS) method—occurrences of the magnitude cutoff (M_{co}) identified as the main discontinuity obtained for the observed catalog through 3000 bootstrap samples.

detected. Figure 6 shows the reconstruction of the FMD model performed by the EMR method. The choice of the normal cumulative distribution function is based on visual inspection and modeling of a variety of catalogs, as well as comparisons to other possible functions, but is not based on physical reasoning. Thus, cases exist for which the choice of another function might be more appropriate. However, synthetic tests endorse that estimates of M_c can be correct even if this assumption is violated (Woessner and Wiemer, 2005). The probability of detecting an earthquake with magnitude M_w, given a specific detectability level determined by the parameters μ and σ, can be quantified by the following function:

$$q(M|\mu,\sigma) = \frac{1}{\sigma\sqrt{2\pi}} \int_{-\infty}^{M_c} \exp\left(-\frac{(M-\mu)^2}{2\sigma^2}\right) dM \quad \text{for } M < M_c, \tag{12}$$

$$q(M|\mu,\sigma) = 1 \quad \text{for } M \geq M_c. \tag{13}$$

The parameter μ represents the magnitude at which 50% of the earthquakes are detected. The parameter σ represents the standard deviation, reflecting the width of the magnitude range over which partial detection occurs. A larger σ corresponds to a wider range of magnitudes over which the detection capability gradually changes. By explicitly incorporating M_c into the equations (12) and (13), as proposed by the authors, the EMR method enables completeness estimation through the

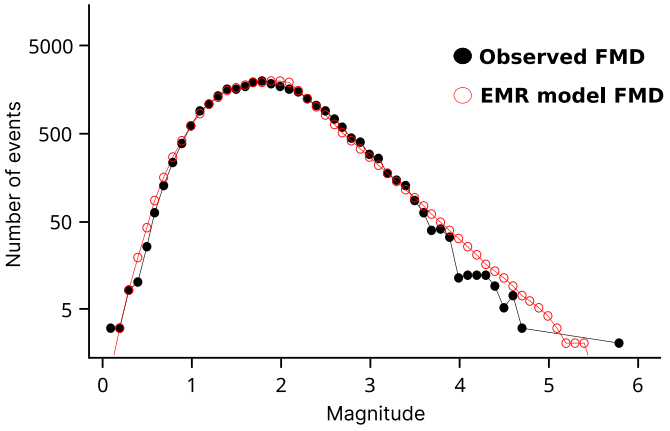

Figure 6. Observed and predicted incremental FMD. The parameters of the EMR model were obtained through maximum-likelihood ($b = 0.93$, $\mu = 1.06$, $\sigma = 0.33$). The color version of this figure is available only in the electronic edition.

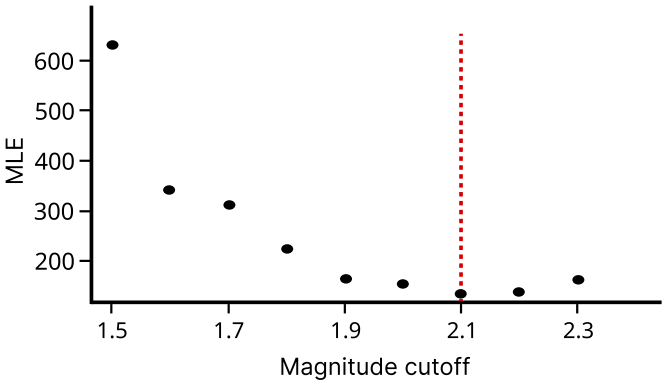

Figure 7. EMR method: maximum-likelihood estimate (MLE) of the completeness magnitude M_c. The EMR fit statistic is evaluated over candidate magnitude cutoffs; it decreases to a distinct minimum at 2.1 (dashed vertical line), so it is selected as the M_c because it provides the best fit (lowest-misfit). The color version of this figure is available only in the electronic edition.

minimization of maximum-likelihood function (Fig. 7). This statistical technique aims to identify the values of the parameters (μ and σ) that maximize the likelihood of observing the seismicity data.

Magnitude of completeness by *b*-value stability

The magnitude of completeness by b-value stability (MBS), initially proposed by Cao and Gao (2002) and further developed by Woessner and Wiemer (2005), offers an approach to estimate the completeness magnitude based on the stability of the b-value with respect to the cutoff magnitude (M_{co}). The MBS method operates under the assumption that the b-value estimates exhibit an increasing trend for M_{co}-values lower than

M_c and remain constant for M_{co}-values greater than or equal to M_c. Deviations from this trend indicate inaccurate b-value estimates when M_{co} is below M_c. Because M_{co} approaches M_c, the b-value converges to its true value and plateaus, reflecting the stable seismicity characteristics. In the original formulation, M_c was arbitrarily defined as the magnitude at which the change in b-value between successive magnitude bin is <0.03. However, Woessner and Wiemer identified the instability of this criterion due to variations in the frequency of events within individual magnitude bins. To address this instability and introduce an objective measure, they proposed using the b-value uncertainty (δb) as the criterion. The b-value uncertainty, originally introduced by Shi and Bolt (1982), is computed as depicted in equation (14):

$$\delta b = 2.3b^2 \sqrt{\frac{\sum_{i=1}^{N}(M_i - \overline{M})^2}{N(N-1)}}. \quad (14)$$

As displayed in equation (14) b represents the estimated b-value, $\overline{M}$ is the mean magnitude, N denotes the number of events, and Mi represents individual cutoff magnitudes. This formulation stabilizes the MBS method numerically. According to the MBS method, M_c is defined as the first magnitude increment at which the absolute difference between the average b-value (bave) and the individual b-value (b) is less than or equal to the b-value uncertainty (δb). The bave is calculated by averaging the b-values of successive cutoff magnitudes within a half magnitude range ($dM = 0.5$) using a bin size of 0.1 (Mignan and Woessner, 2012). The MBS method aims to identify M_c by monitoring the changes in the b-value as M_{co} increases (Fig. 8). When completeness is reached, the b-value exhibits a decline for smaller magnitudes, indicating a shift in earthquake occurrence patterns. Compared with other techniques, the MBS method tends to yield higher M_c-values, as evidenced in the findings presented by Woessner and Wiemer (2005) along with the greater uncertainty.

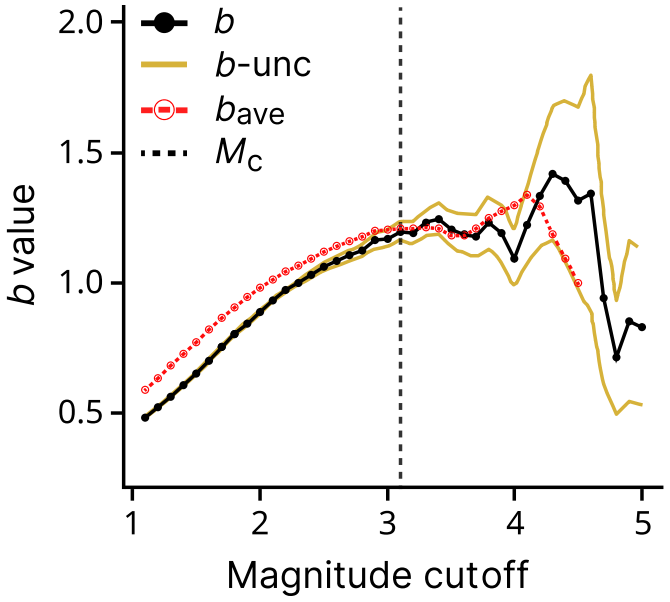

Figure 8. Magnitude of completeness by b-value stability (MBS) method: b-value estimate as a function of minimum magnitude cutoff (M_{co}) with the relate uncertainty. The black circles are used for individual b-values, yellow bands for the uncertainty, and red circles for the b-value average trend. A vertical line marks as M_c (vertical dashed line) the first magnitude increment at which the condition $\Delta b \leq \delta b$ is met. The color version of this figure is available only in the electronic edition.

Evaluating bias in M_c estimation methods for curved datasets

To further investigate the bias of magnitude of completeness estimation methods in case of curved datasets, synthetic catalogs were generated on the ERF model assumptions (Ringdal, 1975; Ogata and Katsura, 2006) for different parameter sets and the M_c estimation was computed. The parameters were varied systematically to span a broad range of potential real-word scenarios, covering integer μ-values from 1 to 3, whereas σ-values ranging from 0.1 to 3.0 with the increments being in steps of 0.1. To ensure the simulations accurately reflected the logarithmic relationship between earthquake magnitude and frequency as mandated by the Gutenberg–Richter law, the b-value was set to 1. To assess the sensitivity of the Gutenberg–Richter slope β to the completeness threshold, we first estimated M_c and quantified its uncertainty via bootstrap resampling. We then took the bootstrap mean of M_c as a baseline and defined a sequence of increasingly conservative thresholds by adding multiples of the M_c standard deviation. For each threshold, β was re-estimated by maximum likelihood using only events above that cutoff (Aki, 1965; Mignan, 2019a). The results across the two models (and both catalog sizes) show that the methods differ in performance depending on the underlying FMD shape, and visual inspection can assist in evaluating the reasonability of a method (Mignan and Woessner, 2012; Mignan and Chen, 2016).

Given the extensive set of simulation, we focus on reporting two representative parameter sets. The first uses the EMR detection parameters for our dataset ($\mu = 1.06$, $\sigma = 0.33$); the second adopts a curved-FMD configuration ($\mu = 2.0$, $\sigma = 0.5$) that better reflects the observed catalog (Fig. 9, panels a–d). Through such analysis, it becomes apparent whether certain techniques are better suited for particular types of seismic activities or specific regions and how the complexities of real-world data impact M_c accuracy (Mignan, 2012). The simulation test was primarily focused on MAXC, GFT, and MBASS. The exclusion of the EMR method from this analysis stems from its fundamental assumption of a normal distribution for the incomplete segment of the dataset, which directly corresponds to the simulated parameters (μ, σ). On the contrary, a comparison between EMR model and a synthetic catalog built on different μ and σ may provide insight on the performance of

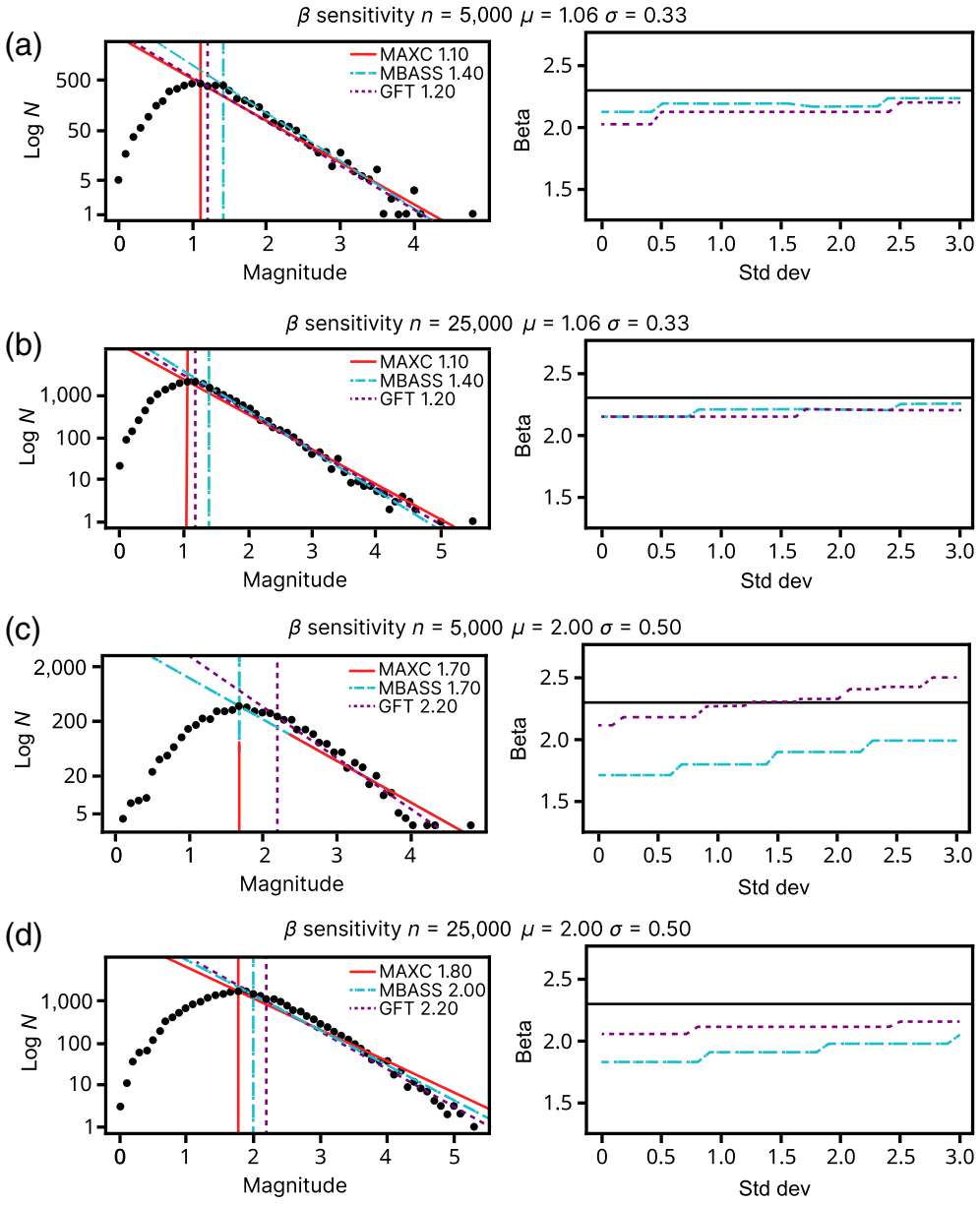

Figure 9. Curved-FMD simulations based on the bulk FMD model of Ringdal (1975). Panels (a,b) use $\mu = 1.06$, $\sigma = 0.33$, and panels (c,d) use $\mu = 2.0$, $\sigma = 0.50$, each with $N = 5{,}000$ and 25,000 events. Left panels: FMDs with completeness estimates M_c with maximum curvature (MAXC) (solid red), MBASS (dotted–dashed cyan), GFT (dashed purple). Right panels: sensitivity of the GR slope β to M_c. The horizontal black line indicates the theoretical value β_{true} used in the simulations, and the cyan and purple curves show β estimated with M_c set to the MBASS and GFT completeness estimates, perturbed by k standard deviations above their bootstrap mean (x-axis label "Std dev" gives k). In all cases, β is the GR slope ($\beta = b \ln 10$) estimated by maximum likelihood for $M \geq M_c$. The color version of this figure is available only in the electronic edition.

the method. In addition, the MBS method was not considered owing to its notable lack of stability. It has been observed that the MBASS and GFT methods might underestimate or overestimate M_c, particularly on certain magnitude samples. To mitigate this issue, it is advised to use bootstrapping techniques (Efron, 1979; Haukoos and Lewis, 2005).

The technique is useful for analyzing data sets in which prior information is sparse, distributional assumptions are unclear, and further data may be difficult to acquire (Henderson, 2005). Adopting a cautious stance involves using the mean plus one to three standard deviations, enhancing the reliability of M_c estimation in the context of curved FMDs (Mignan and Woessner, 2012).

RESULTS AND DISCUSSION

Bootstrap results (3000 resamples) are presented in Figure 10, which summarizes the FMDs for the observed catalog and for all declustered catalogs considered. For each panel, the incremental FMD is shown together with the bootstrap-based magnitude of completeness estimates obtained with all methods adopted in this work (MAXC, MBASS, EMR, GFT, and MBS), reported as color-coded vertical bars. The numerical M_c-values and related uncertainties are reported, in method order, in Tables 2–6.

The completeness magnitude estimated using the MAXC method remains <2.0 for the observed catalog and for all declustered catalogs, with the exception of the one generated using the nearest-neighbor algorithm (Table 2). The Reasenberg and Uhrhammer declustered catalogs, which retain the largest proportion of events, reproduce the observed catalog's completeness around 1.8–1.9. Catalogs declustered with the Gardner–Knopoff and Gruenthal windows show a slight increase in M_c, although values remain <2.0 despite substantial differences in event counts. Notably, the nearest-neighbor catalog yields a higher M_c of 2.1, despite retaining a similar number of events as Gardner–Knopoff windows and far more than Gruenthal windows. Because MAXC identifies the mode of the incremental FMD, this outcome suggests that nearest neighbor preferentially removes earthquakes <2.1, thereby shifting the modal bin to higher magnitudes because of its distinct declustering approach.

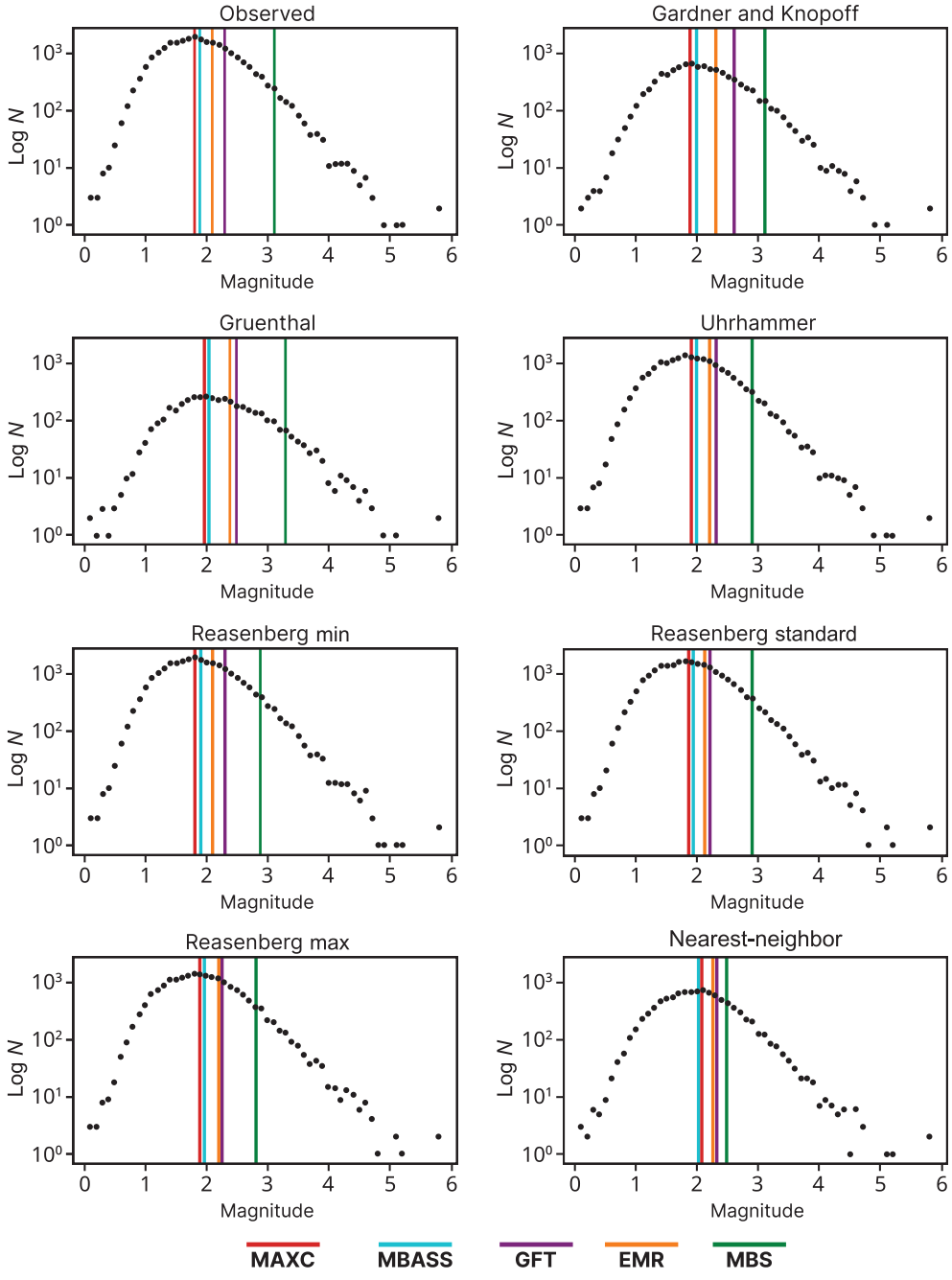

Figure 10. Incremental FMDs for the observed catalog and for all declustered catalogs considered. Color vertical bars indicate the bootstrap-based (3000 resamples) completeness estimates obtained with the catalog-based methods employed: MAXC (red), MBASS (cyan), GFT (purple), EMR (orange), and MBS (green).

The MBASS method defines completeness as the first statistically significant break in the slope of the incremental FMD. The similarity in the results between the MBASS and MAXC methods necessitates cautious interpretation (Tables 2 and 3), particularly in light of MAXC's tendency to underestimate M_c in gradually curved FMD (Mignan 2012). Because it consists of an iterative procedure, it has shown a higher uncertainty. It is worth to note that the MBASS results for the nearest-neighbor declustered catalog show roughly half the uncertainty compared with other declustering algorithms. Single-run MBASS tend to be more variable: estimates reach ~2.1 for Reasenberg and Gardner and Knopoff and reach the peak at 2.3 for Gruenthal. After bootstrap resampling, the observed catalog and those declustered with the Reasenberg, Uhrhammer, and Gardner–Knopoff algorithms show similar results ($M_c < 2.0$). Compared with the MAXC method, the MBASS method showed less sensitivity to the declustering. The Gruenthal and nearest-neighbor methods align, with both catalogs giving slightly higher M_c estimates about 2.0–2.1, even though Gruenthal declustered catalog has <50% of events.

The EMR method M_c results are higher than those of both the MAXC and MBASS methods as illustrated in Table 4. The observed catalog and those declustered with the Reasenberg and Uhrhammer approaches return M_c-values between 2.1 and 2.2. In contrast, the Gardner–Knopoff and nearest-neighbor algorithms achieve 2.3, and the Gruenthal catalog reaches 2.4. Contrary to the results of the MAXC method, it is observed a similarity between Gardner–Knopoff and nearest-neighbor methods despite significant differences in event count. This suggests that EMR is less influenced by which magnitudes are removed than by the total number of events. Single-run and bootstrap estimates coincide across all catalogs, indicating a stable performance. Although the EMR method models the incomplete part of the FMD, the observed discrepancies between synthetic and real catalogs underscore limitations in its effectiveness for defining detection thresholds. The authors recommend caution in its use because of its limited reliability and theoretical foundation (Mignan and Woessner, 2012).

The GFT and MBS methods produced the most conservative estimates of M_c obtained in this study, along with

TABLE 2
Completeness Magnitude (M_c) Estimates and b-Values (with Standard Deviations $M_{c_{sd}}$, b_{sd}) for Each Catalog Using the Maximum Curvature (MAXC) Method

Catalog	nboot	M_c	$M_{c_{sd}}$	b	b_{sd}	Events
Observed	Single-run	1.80	—	0.880	—	26,300
Observed	500	1.85	0.022	0.876	0.032	26,300
Observed	3,000	1.85	0.022	0.876	0.033	26,300
Gruenthal	Single-run	1.90	—	0.590	—	4,226
Gruenthal	500	1.96	0.110	0.626	0.039	4,226
Gruenthal	3,000	1.96	0.115	0.626	0.041	4,226
Gardner and Knopoff	Single-run	1.80	—	0.730	—	9,498
Gardner and Knopoff	500	1.90	0.094	0.733	0.024	9,498
Gardner and Knopoff	3,000	1.91	0.099	0.731	0.026	9,498
Nearest neighbor	Single-run	2.10	—	0.840	—	10,188
Nearest neighbor	500	2.09	0.092	0.868	0.053	10,188
Nearest neighbor	3,000	2.10	0.084	0.871	0.051	10,188
Uhrhammer	Single-run	1.80	—	0.850	—	18,847
Uhrhammer	500	1.85	0.020	0.849	0.020	18,847
Uhrhammer	3,000	1.85	0.022	0.849	0.020	18,847
Reasenberg max	Single-run	1.80	—	0.840	—	19,945
Reasenberg max	500	1.85	0.021	0.842	0.021	19,945
Reasenberg max	3,000	1.85	0.025	0.841	0.022	19,945
Reasenberg standard	Single-run	1.80	—	0.870	—	22,981
Reasenberg standard	500	1.85	0.023	0.863	0.032	22,981
Reasenberg standard	3,000	1.85	0.020	0.865	0.028	22,981
Reasenberg min	Single-run	1.80	—	0.880	—	25,316
Reasenberg min	500	1.84	0.024	0.873	0.036	25,316
Reasenberg min	3,000	1.84	0.026	0.873	0.038	25,316

Results are shown for single-run and bootstrap replicates (500 and 3000).

TABLE 3
Completeness Magnitude (M_c) Estimates and b-Values (with Standard Deviations $M_{c_{sd}}$, b_{sd}) for Each Catalog Using the Median-Based Analysis of the Segment Slope Method (MBASS) Method

Catalog	nboot	M_c	$M_{c_{sd}}$	b	b_{sd}	Events
Observed	Single-run	1.80	—	0.800	—	26,300
Observed	500	1.89	0.137	0.841	0.060	26,300
Observed	3,000	1.90	0.143	0.845	0.063	26,300
Gruenthal	Single-run	2.30	—	0.730	—	4,226
Gruenthal	500	2.02	0.188	0.652	0.061	4,226
Gruenthal	3,000	2.01	0.187	0.648	0.060	4,226
Gardner and Knopoff	Single-run	2.10	—	0.790	—	9,498
Gardner and Knopoff	500	1.97	0.152	0.747	0.061	9,498
Gardner and Knopoff	3,000	1.96	0.150	0.745	0.061	9,498
Uhrhammer	Single-run	1.80	—	0.770	—	18,847
Uhrhammer	500	1.95	0.154	0.847	0.071	18,847
Uhrhammer	3,000	1.96	0.155	0.848	0.071	18,847
Nearest neighbor	Single-run	2.10	—	0.900	—	10,188
Nearest neighbor	500	2.06	0.088	0.882	0.048	10,188
Nearest neighbor	3,000	2.06	0.090	0.881	0.049	10,188
Reasenberg max	Single-run	2.10	—	0.900	—	19,945
Reasenberg max	500	1.92	0.143	0.824	0.063	19,945
Reasenberg max	3,000	1.92	0.142	0.825	0.062	19,945
Reasenberg standard	Single-run	1.80	—	0.790	—	22,981
Reasenberg standard	500	1.92	0.146	0.843	0.065	22,981
Reasenberg standard	3,000	1.92	0.144	0.845	0.064	22,981
Reasenberg min	Single-run	1.80	—	0.800	—	25,316
Reasenberg min	500	1.90	0.144	0.843	0.064	25,316
Reasenberg min	3,000	1.89	0.141	0.841	0.063	25,316

Results are shown for single-run and bootstrap replicates (500 and 3000).

TABLE 4
Completeness Magnitude (M_c) Estimates and *b*-Values (with Standard Deviations $M_{c_{sd}}$, b_{sd}) for Each Catalog Using the Entire Magnitude Range (EMR) Method

Catalog	nboot	M_c	$M_{c_{sd}}$	*b*	b_{sd}	Events
Observed	Single-run	2.10	—	0.930	—	26,300
Observed	500	2.12	0.044	0.941	0.020	26,300
Observed	3,000	2.13	0.044	0.943	0.021	26,300
Gruenthal	Single-run	2.40	—	0.760	—	4,226
Gruenthal	500	2.35	0.069	0.749	0.025	4,226
Gruenthal	3,000	2.36	0.069	0.750	0.026	4,226
Gardner and Knopoff	Single-run	2.30	—	0.860	—	9,498
Gardner and Knopoff	500	2.30	0.037	0.869	0.020	9,498
Gardner and Knopoff	3,000	2.30	0.037	0.868	0.020	9,498
Nearest neighbor	Single-run	2.30	—	0.980	—	10,188
Nearest neighbor	500	2.29	0.042	0.979	0.024	10,188
Nearest neighbor	3000	2.30	0.038	0.980	0.022	10,188
Uhrhammer	Single-run	2.20	—	0.950	—	18,847
Uhrhammer	500	2.19	0.025	0.950	0.015	18,847
Uhrhammer	3,000	2.19	0.026	0.950	0.015	18,847
Reasenberg max	Single-run	2.20	—	0.930	—	19,945
Reasenberg max	500	2.18	0.039	0.931	0.018	19,945
Reasenberg max	3,000	2.18	0.036	0.932	0.017	19,945
Reasenberg standard	Single-run	2.10	—	0.920	—	22,981
Reasenberg standard	500	2.16	0.050	0.944	0.021	22,981
Reasenberg standard	3,000	2.15	0.050	0.943	0.022	22,981
Reasenberg min	Single-run	2.10	—	0.930	—	25,316
Reasenberg min	500	2.14	0.048	0.948	0.023	25,316
Reasenberg min	3,000	2.14	0.048	0.947	0.023	25,316

Results are shown for Single-Run and bootstrap replicates (500 and 3000).

high uncertainty values (Tables 5 and 6). The GFT results range between 2.2 and 2.7, the second highest M_c estimations of the entire study. In both single-run and bootstrap computations, the catalogs declustered with the Reasenberg, Uhrhammer, and nearest-neighbor approaches match the observed catalog M_c of 2.3. Cases of under- or overestimation arise only in two fixed-window approaches used. For the catalog declustered with the Gardner and Knopoff algorithm, the single GFT run yields 2.7, but the bootstrap stabilizes the estimate around 2.5. Same bootstrap results are achieved for the Gruenthal declustered catalog, but resampling raises the single run M_c initial estimation of 2.3. The application of the GFT provides valuable insights into the alignment of the observed seismic data with the expected statistical distribution according to the Gutenberg–Richter law. This alignment or lack thereof can help understanding the representativeness of our catalog in capturing the range of seismic activities. As a matter of fact, it is also used as indirect assessment of upgrades in the seismic network. Despite the well-known limit of selecting the first M_{co} that achieves the test statistic, the results offer a good compromise between managing undersampling and being conservative. It appears reasonable to consider slightly higher value of the M_{co} that demonstrate improved performance in statistical testing as completeness.

The MBS method gives the most conservative completeness and shows the widest separation across declustering choices (Table 6). Initially, the computation failed to identify the completeness for the observed catalog: the range of potential values adopted from (Mignan and Woessner, 2012) was centered around the value of MAXC (1.8 for the observed catalog), resulting in a maximum and minimum value of M_{co} of 1.1 and 3.0, respectively. After expanding the range of potential completeness values from 20 to 40, MBS immediately identified M_c above 3.0, confirming the initial suspicion and demonstrating that caution should be exercised in defining the values of M_{co} to be tested when applying this methodology. When the number of events is slightly reduced, as in the catalogs declustered with the Uhrhammer and Reasenberg algorithms, the MBS recorded lower results. In contrast, the catalogs declustered with Gardner and Knopoff and Gruenthal windows, which are more aggressive, yield higher M_c estimates. The nearest-neighbor catalog is a special case. Although its number of events is comparable to the Gardner and Knopoff declustered catalog, the single run overestimates M_c at 2.6, and the bootstrap stabilizes at just <2.5, making it distinctly lower than all other catalogs.

The Gutenberg–Richter *b*-value varies systematically with declustering aggressiveness and the fraction of events retained.

TABLE 5
Completeness Magnitude (M_c) Estimates and b-Values (with Standard Deviations $M_{c_{sd}}$, b_{sd}) for Each Catalog Using the Goodness-of-Fit Test (GFT) Method

Catalog	nboot	M_c	$M_{c_{sd}}$	b	b_{sd}	Events
Observed	Single-run	2.30	—	0.990	—	26,300
Observed	500	2.34	0.123	1.015	0.042	26,300
Observed	3,000	2.35	0.127	1.017	0.042	26,300
Gruenthal	Single-run	2.30	—	0.730	—	4,226
Gruenthal	500	2.52	0.276	0.808	0.092	4,226
Gruenthal	3,000	2.53	0.271	0.811	0.091	4,226
Gardner and Knopoff	Single-run	2.70	—	0.970	—	9,498
Gardner and Knopoff	500	2.54	0.249	0.942	0.082	9,498
Gardner and Knopoff	3,000	2.56	0.250	0.946	0.082	9,498
Nearest neighbor	Single-run	2.30	—	0.980	—	10,188
Nearest neighbor	500	2.34	0.080	0.994	0.033	10,188
Nearest neighbor	3,000	2.34	0.084	0.995	0.034	10,188
Uhrhammer	Single-run	2.30	—	0.970	—	18,847
Uhrhammer	500	2.28	0.102	0.976	0.033	18,847
Uhrhammer	3,000	2.28	0.106	0.978	0.033	18,847
Reasenberg max	Single-run	2.20	—	0.930	—	19,945
Reasenberg max	500	2.23	0.060	0.947	0.020	19,945
Reasenberg max	3,000	2.24	0.065	0.947	0.021	19,945
Reasenberg standard	Single-run	2.20	—	0.950	—	22,981
Reasenberg standard	500	2.24	0.060	0.972	0.021	22,981
Reasenberg standard	3,000	2.24	0.064	0.971	0.023	22,981
Reasenberg min	Single-run	2.30	—	1.000	—	25,316
Reasenberg min	500	2.29	0.094	1.000	0.031	25,316
Reasenberg min	3,000	2.29	0.105	1.003	0.035	25,316

Results are shown for single-run and bootstrap replicates (500 and 3000).

Fixed-window methods (Gruenthal and Gardner and Knopoff), which retain roughly 15%–35% of the events, yield the strongest depressions in b-value (typically in range 0.10–0.25). For example, relative to the observed catalog, under MAXC, an initial b-value equal to 0.88 drops to 0.73 with Gardner and Knopoff and to 0.62 with Gruenthal; with EMR, the b-value decreases from 0.94 to 0.75. Milder fixed-windowing (Uhrhammer), retaining ~70%, preserves b-value close to the observed catalog. The Reasenberg (all configuration, between 75% and 95% retained) b-value results mimic the observed catalog, indicating minimal distortion of the magnitude–frequency slope. The nearest-neighbor approach (40% retained) shows M_c method–dependent behavior: small increases under EMR and MBASS and small decreases for MAXC and GFT but and a more marked drop under MBS (0.17). Because b governs the relative weight of larger magnitudes, even modest shifts are consequential for long-return-period hazard (Marzocchi and Taroni, 2014; Teng and Baker, 2019; Taroni and Akinci, 2021).

CONCLUSIONS

Catalog-based methods offer a simple instrumental approach to compute M_c estimations. They are time-saving and easy to implement; the computation involves only the magnitude vector to infer the completeness from the expected behavior of seismicity (Mignan and Woessner, 2012). Given the observed catalog, starting with a simpler method such as MAXC for an initial estimation of M_c could be practical, especially when the FMD shows a gradual curve (Mignan and Woessner, 2012). This method provides a baseline understanding of seismic completeness, setting the stage for more detailed analyses. The MAXC technique offers several advantages that make it time-saving and easy to handle. First, it relies on simple mathematical assumptions, specifically the calculation of derivatives. This makes it computationally efficient and relatively straightforward to implement. Second, even though MAXC tends to underestimate systematically M_c in case of gradual curved shape FMD (Mignan and Woessner, 2012), it is widely used as starting point to define the range of the potential completeness magnitudes for other methods.

The use of resampling techniques has proven to be highly effective. By resampling the catalog data, it was possible to assess the stability and uncertainty of completeness estimates. Even with a minimum bootstrap value, the completeness results remained stable. Different methods offer varied analytical perspective of M_c, emphasizing that no single approach is universally applicable. Therefore, choosing the appropriate methodology must be contingent on the intended purpose of the study, ensuring that the assessment of M_c aligns with the context and the unique geological features of the region under investigation.

TABLE 6
Completeness Magnitude (M_c) Estimates and *b*-Values (with Standard Deviations $M_{c_{sd}}$, b_{sd}) for Each Catalog Using the Magnitude of Completeness by the *b*-Value Stability (MBS) Method

Catalog	nboot	M_c	$M_{c_{sd}}$	*b*	b_{sd}	Events
Observed	Single-run	3.10	—	1.19	—	26,300
Observed	500	3.06	0.152	1.201	0.057	26,300
Observed	3,000	3.05	0.165	1.201	0.067	26,300
Gruenthal	Single-run	3.40	—	1.04	—	4,226
Gruenthal	500	3.27	0.312	1.073	0.253	4,226
Gruenthal	3,000	3.29	0.313	1.084	0.299	4,226
Gardner and Knopoff	Single-run	3.10	—	1.08	—	9,498
Gardner and Knopoff	500	3.15	0.258	1.136	0.187	9,498
Gardner and Knopoff	3,000	3.15	0.278	1.140	0.281	9,498
Nearest neighbor	Single-run	2.60	—	1.06	—	10,188
Nearest neighbor	500	2.47	0.276	1.022	0.106	10,188
Nearest neighbor	3,000	2.48	0.274	1.024	0.104	10,188
Uhrhammer	Single-run	2.90	—	1.11	—	18,847
Uhrhammer	500	2.92	0.185	1.128	0.055	18,847
Uhrhammer	3,000	2.94	0.191	1.134	0.062	18,847
Reasenberg max	Single-run	2.90	—	1.07	—	19,945
Reasenberg max	500	2.85	0.297	1.088	0.126	19,945
Reasenberg max	3,000	2.84	0.264	1.082	0.088	19,945
Reasenberg standard	Single-run	2.90	—	1.10	—	22,981
Reasenberg standard	500	2.94	0.257	1.131	0.082	22,981
Reasenberg standard	3,000	2.94	0.262	1.129	0.085	22,981
Reasenberg min	Single-run	2.90	—	1.14	—	25,316
Reasenberg min	500	2.94	0.177	1.156	0.050	25,316
Reasenberg min	3,000	2.94	0.179	1.160	0.057	25,316

Results are shown for single-run and bootstrap replicates (500 and 3000).

The range of M_c-values obtained from different techniques may not always overlap. Such discrepancies arise because these methods do not necessarily adhere to a uniform definition of M_c (Mignan and Woessner, 2012). In summing up the findings of the study, it is crucial to acknowledge that even when a particular technique yields a low uncertainty estimate for the magnitude of completeness, it does not inherently affirm the reliability of the estimation itself. Rather, it suggests that the estimated output is robust within the context of the dataset analyzed. Declustering may have a direct impact on M_c estimation: more aggressive algorithms tend to remove proportionally more small events and can shift M_c upward, which in turn depresses the Gutenberg–Richter *b*-value (Mizrahi *et al.*, 2021; Taroni and Akinci, 2021; Pavlenko and Zavyalov, 2022; Bi *et al.*, 2024).

Lowering the number of events did not always produce more conservative M_c estimates, suggesting the influence of the shape of the FMD and the assumptions of the method used. Using the Gardner and Knopoff declustering algorithm, the MBS completeness results differ markedly from that obtained with nearest-neighbor declustered catalog, which removed a similar number of events yet yield a clearly lower estimate. This contrast shows that changes are driven more by "where" and "how" events are removed than by how many. Declustering often removes earthquakes from high-productivity, high-sensitivity subregions. Considering the entire catalog, these areas contribute many small events that depress the apparent completeness and mask the higher completeness of less sensitive regions. Although waveform overlap after mainshocks briefly suppresses detection of small events, the spatial heterogeneity persists much longer. A successive step may be based on grid M_c method, including the Bayesian approach described by Mignan *et al.* (2011), to quantify it.

DATA AND RESOURCES

The earthquake catalog used in this study was obtained from the Italian National Institute of Geophysics and Volcanology (Istituto Nazionale di Geofisica e Vulcanologia, INGV) through the ISIDe database (ISIDe Working Group, INGV, doi: 10.13127/ISIDe).

DECLARATION OF COMPETING INTERESTS

The authors acknowledge that there are no conflicts of interest recorded.

ACKNOWLEDGMENTS

The authors thank the two anonymous reviewers for their thoughtful and constructive feedback. Their insights guided the revisions and helped the authors refine the presentation and interpretation of the work. The authors believe these changes have enhanced the article's clarity and coherence.

REFERENCES

Abd el-aal, A. E. (2012). Very broadband seismic background noise analysis of permanent good vaulted seismic stations, *J. Seismol.* **17,** doi: 10.1007/s10950-012-9308-5.

Abercrombie, R. E. (1995). Earthquake source scaling relationships from -1 to 5 ML using seismograms recorded at 2.5 km depth, *J. Geophys. Res. Solid Earth* **100,** no. B12, 24,015–24,036.

Aki, K. (1965). Maximum likelihood estimate of b in the formula log N=a-bM and its confidence limits, *Bull. Earthq. Res. Inst. Univ. Tokyo* **43,** 237.

Amini, H. (2014). Comparing Reasenberg and Gruenthal Declustering Methods for North of Iran, *Proc. of the Second European Conf. on Earthquake Engineering and Seismology (2ECEES)*, Istanbul, Türkiye, 25–29 August 2014.

Amorese, D. (2007). Applying a change-point detection method on frequency-magnitude distributions, *Bull. Seismol. Soc. Am.* **97,** no. 5, 1742–1749, doi: 10.1785/0120060181.

Azak, T., D. Kalafat, K. Şeşetyan, and M. B. Demircioğlu (2018). Effects of seismic declustering on seismic hazard assessment: A sensitivity study using the Turkish earthquake catalogue, *Bull. Earthq. Eng.* **16,** no. 8, 3339–3366, doi: 10.1007/s10518-017-0174-y.

Bi, J., C. Song, and F. Cao (2024). Declustering characteristics of the North China Plain seismic belt and its effect on probabilistic seismic hazard analysis, *Sci. Rep.* **14,** no. 1, 22,170, doi: 10.1038/s41598-024-73815-9.

Cao, A. M., and S. S. Gao (2002). Temporal variations of seismic b-values beneath northeastern japan island arc, *Geophys. Res. Lett.* **29,** 48-1.

Cornell, C. A. (1968). Engineering seismic risk analysis, *Bull. Seismol. Soc. Am.* **58,** no. 5, 1583–1606, doi: 10.1785/BSSA0580051583.

D'Alessando, A., L. Greco, S. Scudero, and V. Lauciani (2021). Spectral characterization and spatiotemporal variability of the background seismic noise in Italy, *Earth Space Sci.* **8,** doi: 10.1029/2020EA001579.

Efron, B. (1979). Bootstrap methods: Another look at the jackknife, *Ann. Stat.* **7,** no. 1, 1–26, doi: 10.1214/aos/1176344552.

Gardner, J. K., and L. Knopoff (1974). Is the sequence of earthquakes in southern California, with aftershocks removed, Poissonian? *Bull. Seismol. Soc. Am.* **64,** 1363–1367.

Gomberg, J. (1991). Seismicity and detection/location threshold in the southern Great Basin seismic network, *J. Geophys. Res. Solid Earth* **96,** no. B10, 16,401–16,414.

Gonzalez, A. (2017). The Spanish National Earthquake catalogue: Evolution, precision and completeness, *J. Seismol.* **21,** no. 3, 435–471, doi: 10.1007/s10950-016-9610-8.

Gutenberg, B., and C. F. Richter (1944). Frequency of earthquakes in California, *Bull. Seismol. Soc. Am.* **34,** no. 4, 185–188, doi: 10.1785/BSSA0340040185.

Haukoos, J. S., and R. J. Lewis (2005). Advanced statistics: Bootstrapping confidence intervals for statistics with "difficult" distributions, *Acad. Emerg. Med.* **12,** no. 4, 360–365, doi: 10.1197/j.aem.2004.11.018.

Helmstetter, A., Y. Y. Kagan, and D. D. Jackson (2006). Comparison of short-term and time-independent earthquake forecast models for southern California, *Bull. Seismol. Soc. Am.* **96,** no. 1, 90–106.

Henderson, A. R. (2005). The bootstrap: A technique for data-driven statistics, *Clin. Chim. Acta* **359,** nos. 1/2, 1–26, doi: 10.1016/j.cccn.2005.04.002.

Hollander, M., and D. A. Wolfe (1973). *Nonparametric Statistical Methods*, John Wiley & Sons, New York.

Huang, W. Q., W. X. Li, and X. F. Cao (1994). Completeness analysis of earthquake catalogs in China Main Land II, *Acta Seismol. Sin.* **7,** no. 4, 529–538.

Ishimoto, M., and K. Iida (1939). Observations of earthquakes registered with the microseismograph constructed recently, *Bull. Earthq. Res. Inst.* **17,** 443–478.

Juellyan, J., B. Setiawan, M. Hasan, H. Yunita, M. Sungkar, and T. Saidi (2023). Comparing Gardner-Knopoff, Gruenthal, and Uhrhammer earthquake declustering methods in Aceh, Indonesia, *IOP Conf. Ser.* **1245,** 012010.

Kagan, Y. Y. (2004). Short-term properties of earthquake catalogs and models of earthquake source, *Bull. Seismol. Soc. Am.* **94,** no. 4, 1207–1228, doi: 10.1785/012003098.

Kanamori, H., and D. L. Anderson (1975). Theoretical basis of some empirical relations in seismology, *Bull. Seismol. Soc. Am.* **65,** no. 5, 1073–1095.

Lanzante, J. R. (1996). Resistant, robust and non-parametric techniques for the analysis of climate data, *Int. J. Climatol.* **16,** 1197–1226.

Liu, J., Q. F. Chen, and Y. Chen (1996). Completeness analysis of the seismic catalog in North China region, *Earthquake* **16,** no. 1, 59–67.

Luen, B., and P. B. Stark (2012). Poisson tests of declustered catalogues, *Geophys. J. Int.* **189,** no. 1, 691–700.

Marzocchi, W., and M. Taroni (2014). Some thoughts on declustering in probabilistic seismic-hazard analysis, *Bull. Seismol. Soc. Am.* **104,** no. 4, 1838–1845, doi: 10.1785/0120130300.

Mignan, A. (2012). Functional shape of the earthquake frequency-magnitude distribution and completeness magnitude, *J. Geophys. Res. Solid Earth* **117,** no. B8, doi: 10.1029/2012JB009347.

Mignan, A. (2019a). rseismNet: Earthquake frequency–magnitude distribution and network statistics, GitHub Repository, available at https://github.com/amignan/rseismNet (last accessed November 2025).

Mignan, A., and C. C. Chen (2016). The spatial scale of detected seismicity, *Pure Appl. Geophys.* **173,** 117–124, doi: 10.1007/s00024-015-1133-7.

Mignan, A., and G. Chouliaras (2014). Fifty years of seismic network performance in Greece (1964–2013), *Seismol. Res. Lett.* **85,** 657–667, doi: 10.1785/0220130209.

Mignan, A., and J. Woessner (2012). Estimating the magnitude of completeness for earthquake catalogs, *Commun. Online Resour. Stat. Seism. Anal.*, 1–45, doi: 10.5078/corssa-00180805.

Mignan, A., M. Werner, S. Wiemer, C. Chen, and Y. Wu (2011). Bayesian estimation of the spatially varying completeness magnitude of earthquake catalogs, *Bull. Seismol. Soc. Am.* **101,** 1371–1385, doi: 10.1785/0120100223.

Mizrahi, L., S. Nandan, and S. Wiemer (2021). The effect of declustering on the size distribution of mainshocks, *Seismol. Res. Lett.* **92,** no. 4, 2333–2342, doi: 10.1785/0220200231.

Molchan, G. M., and O. E. Dmitrieva (1992). Aftershock identification: Methods and new approaches, *Geophys. J. Int.* **109,** no. 3, 501–516.

Ogata, Y., and K. Katsura (1993). Analysis of temporal and spatial heterogeneity of magnitude frequency distribution inferred from earthquake catalogues, *Geophys. J. Int.* **113,** 727–738.

Ogata, Y., and K. Katsura (2006). Immediate and updated forecasting of aftershock hazard, *Geophys. Res. Lett.* **33,** L10305 , doi: 10.1029/2006GL025888.

Pavlenko, V. A., and A. D. Zavyalov (2022). Comparative analysis of the methods for estimating the magnitude of completeness of earthquake catalogs, *Izv. Phys. Solid Earth* **58,** 89–105.

Perry, M., and R. Bendick (2024). A comparative analysis of five commonly implemented declustering algorithms, *J. Seismol.* **28,** no. 3, 829–842, doi: 10.1007/s10950-024-10221-8.

Reasenberg, P. A. (1985). Second-order moment of central California seismicity, 1969–1982, *J. Geophys. Res. Solid Earth* **90,** no. B7, 5479–5495.

Ringdal, F. (1975). On the estimation of seismic detection thresholds, *Bull. Seismol. Soc. Am.* **65,** 1631–1642.

Rydelek, P. A., and I. S. Sacks (1989). Testing the completeness of earthquake catalogs and the hypothesis of self-similarity, *Nature* **337,** 251–253.

Schorlemmer, D., and M. C. Gerstenberger (2007). RELM testing center, *Seismol. Res. Lett.* **78,** no. 1, 30–36, doi: 10.1785/gssrl.78.1.30.

Schorlemmer, D., F. Mele, and W. Marzocchi (2010). A completeness analysis of the National Seismic Network of Italy, *J. Geophys. Res. Solid Earth* **115,** no. B4, doi: 10.1029/2008JB006097.

Schorlemmer, D., S. Wiemer, and M. Wyss (2005). Variations in earthquake-size distribution across different stress regimes, *Nature* **437,** 539–542, doi: 10.1038/nature04094.

Sereno, T. J., Jr., and S. R. Bratt (1989). Seismic detection capability at NORESS and implications for the detection threshold of a hypothetical network in the Soviet Union, *J. Geophys. Res. Solid Earth* **94,** no. B8, 10,397–10,414.

Shi, Y., and B. A. Bolt (1982). The standard error of the magnitude frequency b-value, *Bull. Seism. Soc. Am.* **72,** 1677–1687.

Silva, V., H. Crowley, M. Pagani, D. Monelli, and R. Pinho (2014). Development of the OpenQuake engine, the Global Earthquake Model's open-source software, *Nat. Hazards* **72,** 1409–1427, doi: 10.1007/s11069-013-0618-x.

Taroni, M., and A. Akinci (2021). Good practices in PSHA: Declustering, b-value estimation, foreshocks and aftershocks inclusion, *Geophys. J. Int.* **224,** no. 2, 1174–1187, doi: 10.1093/gji/ggaa462.

Teng, G., and J. W. Baker (2019). Seismicity declustering and hazard analysis of the Oklahoma–Kansas region, *Bull. Seismol. Soc. Am.* **109,** no. 6, 2356–2366.

Uhrhammer, R. (1986). Characteristics of Northern and Central California seismicity, *Earthq. Notes* **57,** no. 1, 21.

Van Stiphout, T., J. Zhuang, and D. Marsan (2012). Seismicity declustering, *Commun. Online Resour. Stat. Seismicity Anal.*, doi: 10.5078/corssa52382934.

Wesnousky, S. G. (1994). The Gutenberg-Richter or characteristic earthquake distribution, which is it? *Bull. Seismol. Soc. Am.* **84,** 1940–1958.

Wiemer, S., and M. Wyss (2000). Minimum magnitude of completeness in earthquake catalogs: Examples from Alaska, the Western United States, and Japan, *Bull. Seismol. Soc. Am.* **90,** no. 4, 859–869.

Wilcoxon, F. (1945). Individual comparisons by ranking methods, *Biometrics Bull.* **1,** 80–83.

Woessner, J., and S. Wiemer (2005). Assessing the quality of earthquake catalogues: Estimating the magnitude of completeness and its uncertainty, *Bull. Seismol. Soc. Am.* **95,** no. 2, 684–698.

Wyss, M., A. Hasegawa, S. Wiemer, and N. Umino (1999). Quantitative mapping of precursory seismic quiescence before the 1989, M7.1 off-Sanriku earthquake, Japan, *Ann. Geophys.* **42,** doi: 10.4401/ag-3765.

Xu, W., and M. Gao (2014). Statistical analysis of the completeness of earthquake catalogs in China mainland, *Chin. J. Geophys.* **57,** no. 9, 2802–2812.

Zaliapin, I., and Y. Ben-Zion (2013a). Earthquake clusters in southern California I: Identification and stability, *J. Geophys. Res. Solid Earth* **118,** no. 6, 2847–2864, doi: 10.1002/jgrb.50179.

Zaliapin, I., and Y. Ben-Zion (2013b). Earthquake clusters in southern California II: Classification and relation to physical properties of the crust, *J. Geophys. Res. Solid Earth* **118,** no. 6, 2865–2877, doi: 10.1002/jgrb.50178.

Zaliapin, I., and Y. Ben-Zion (2020). Earthquake declustering using the nearest-neighbor approach in space-time-magnitude domain, *J. Geophys. Res. Solid Earth* **125,** no. 4, e2018JB017120, doi: 10.1029/2018JB017120.

Zuniga, F. R., and M. Wyss (1995). Inadvertent changes in magnitude reported in earthquake catalogs: Their evaluation through b-value estimates, *Bull. Seismol. Soc. Am.* **85,** 1858–1866.

Manuscript received 6 June 2025
Published online 23 February 2026